Journal of Thermal Analysis, Vol. 45 (1995) 1419-1435

NON-ISOTHERMAL SHORT-RANGE-ORDERING BY EXCESS VACANCIES IN αCu–Zn ALLOYS

E. Donoso and A. Varschavsky

Universidad de Chile, Facultad de Ciencias Físicas y Matemáticas, Departamento de Ingeniería de los Materiales-IDIEM, Casilla 1420, Santiago, Chile

(Received November 21, 1994)

Abstract

The kinetics short-range-order (SRO) in quenched Cu-30 at.%Zn, Cu-25 at.%Zn and Cu-20 at.%Zn was investigated by differential scanning calorimetry (DSC). It was evidenced a growing atomic mobility with increasing Zn content. From the DSC traces it is inferred that ordering is established in one stage, assisted by excess vacancies. As the quenching temperature increases considerable reordering occurs during cooling from the quenching temperature. The variation in the SRO non-isothermal behaviour with quenching temperature and composition is interpreted in terms of the atomic mobility and the degree of disorder together with the concentration of vacancies retained by quenching. Activation energies which control the mean life of vacancies and those which control the ordering rate were very similar, indicating that the mobility of vacancies is highly effective in generating SRO. Such activation energies are somewhat lower than the effective energies which control the kinetics of the process obtained from the DSC traces, suggesting that the presence of solute-vacancy complexes may be important as the Zn concentration increases. This feature was confirmed by an estimation of the solute-vacancy binding energy. It was also inferred that divacancy formation is unlikely in the alloys under study.

Keywords: αCu–Zn alloys, kinetics, short-range-order

Introduction

Changes in the microstructure of the solid solution of Zn in Cu have been studied for some time by resistivity measurements [1, 2], calorimetry [3, 4], X-ray and neutron diffraction [5], and measurements of the lattice parameter [6, 7], and stress relaxation [8, 9]. The existence of short-range order (SRO) near the phase boundary of the α-β' two-phase region is very well established. In contrast to the usual experiments on SRO kinetics after quenching from rather high temperatures Trattner and Pfeiler [10], stated that the adjustment of a new equilibrium state of SRO is established after small and sudden temperature changes. Other authors deduce the existence of SRO from a linear increase in the resistivity (destruction of order) during isochronal annealing [1, 2].

0368–4466/95/ $ 5.00

John Wiley & Sons, Limited
Chichester

Although, one sees that while this alloy system has been rather intensively investigated for a long time, no fully acceptable description of the kind of local order has evolved, the interpretation of the results being strongly influenced by the type of experiments carried out. In addition, although the study of SRO phenomena in αCu–Zn alloys continues [11, 12], there is comparatively little research concerning the kinetics of the SRO process from a quantitative treatment of DSC traces. Besides, no systematic studies concerning quantitative evaluation of ordering phenomena during quenching and reordering until equilibrium is reached have been reported. There is also a need to examine the roll of solute-vacancy complexes and vacancy mobility in the ordering process to the end of explaining the observed features displayed by the differential scanning calorimetry (DSC) traces.

The principal objectives of the present work are: a) to determine whether during non-isothermal experiments performed in quenched alloys a homogeneous rather than a heterogeneous SRO state is developed; b) to determine the kinetics parameters of the ordering reactions and the effect of bounded vacancies; c) to compute boundary values for the first SRO parameter from the features displayed by the DSC traces (thus enabling the capabilities of the technique to be enhanced); d) to examine the effect of quenching temperature; and e) to study the incidence of vacancy mobility and bounded vacancies during the ordering process until equilibrium is attained.

Experimental

The alloys studied were Cu-20 at.%Zn, Cu-25 at.%Zn and Cu-30 at.%Zn. They were prepared in a Baltzer VSG 10 vacuum induction furnace from 99.97% purity electrolytic copper and 99.9% purity zinc in a graphite crucible. The ingots were subsequently hot forged at 923 K to a thickness of 10 mm, pickled to remove oxide from the surface and annealed in a vacuum furnace at 1123 K for 36 h to achieve complete homogeneity and cooled in the furnace to room temperature. The alloys were then cold rolled to 0.75 mm thickness with intermediate annealings at 923 K for 1 h. For solution treatment the samples were heated for 1 h at 873 K, followed by quenching. In order to determine the quenching effects two other selected temperatures (1073 and 673 K) were choosen. Microcalorimetric analysis of the samples was performed in a DuPont 2000 thermal analyzer.

Results and discussion

Differential scanning calorimetry

Typical thermograms for the three alloys are shown in the differential heat capacity ΔC_p *vs.* temperature curves at indicated heating rates Φ in Fig. 1. They

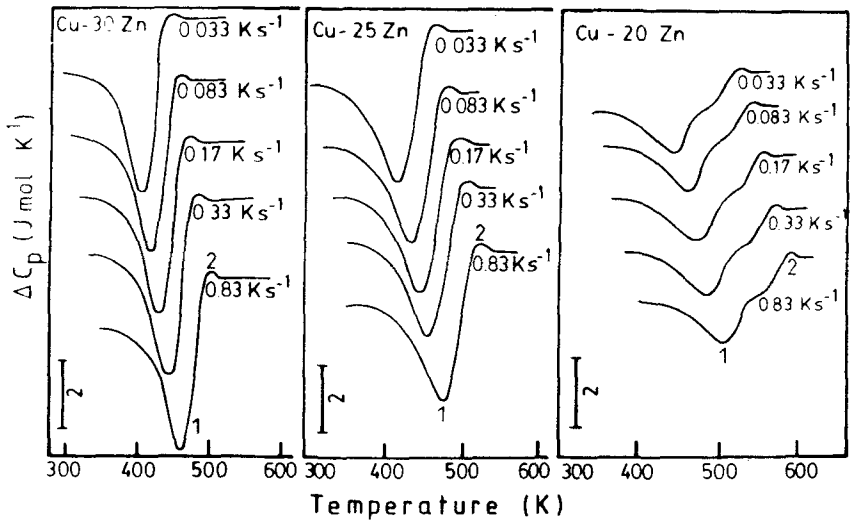

Fig. 1 DSC curves for αCu–Zn alloys quenched from 873 K

are characterized by one exothermic peak, namely stage 1 and one endothermic peak, stage 2. Stage 1 have been reported in the literature in connection with SRO development assisted by migration of excess vacancies, while stage 2 was associated with a disordering process [3, 4]. The height and area under all these peaks increase with increasing zinc content. It can be observed in Fig. 1 that all stages shift to lower temperatures as the zinc concentration increases. Further, the relative dominances of the two stages are independent of the heating rate. These features reflect that both reactions are dominated by kinetic rather than by thermodynamic factors. A kinetically dominated dissolution process is expected for a homogeneous SRO state or from the dissolution of particles taking place by a second-order transition [13]. However, in the latter case, the width and height of stage 2 would be dependent on the heating rate [13]. If the dissolution occurs by a first-order transition as in a DO state in α-brass, where ordered domains are based on the Cu_3Zn structure [3], such a process would be thermodynamically dominated, and hence the peak temperature of stage 2 would be independent of the heating rate. None of these features are observed in Fig. 1. Therefore, the observed heating rate dependence of the peak temperature of stage 2 and its associated shape invariability is in favour of disordering of a homogeneous SRO state.

The areas under the ΔC_p *vs.* T curves which correspond to the enthalpies of the different reactions in stages 1 and 2 are listed in Table 1. The enthalpy absorption associated with stage 2 was evaluated by considering the area of the ΔC_p *vs.* T curve between the temperature at which the curve of stage 1 crosses the baseline, and the temperature at which energy is absorbed at a constant rate

Table 1 Enthalpimetric data for stages 1 and 2 measured at a heating rate $\Phi=0.33$ K/s (Data represent the average of five differential scanning calorimetry runs)

Zn content in the material/ at. %	$-\Delta H_1$ / J·mol^{-1}	ΔH_2 / J·mol^{-1}
30	155±5	58±3
25	130±5	52±3
20	67±3	31±2

from the baseline. It can be noticed that all these enthalpies increase as the alloy becomes more concentrated. It was also verified that their values are independent of the heating rate.

Kinetic parameters and kinetic laws

Values for activation energies are required as a necessary input in order to perform the non-isothermal kinetic analysis. These values were computed from plots of $\ln(\Phi/T_p)$ *vs.* $1/T_p$ (Kissinger's peak shift method [14]) for the stages 1 and 2, where T_p is the peak temperature and Φ the heating rate. These plots of slope $(-E/R)$ resulted in straight lines. They are not shown in the present work for the sake of brevity. The values of the activation energy E for each process, which are listed in Table 2, decrease with increasing zinc content, consistently with the increase in atomic mobility usually found in solid solutions of copper as the solute concentration increases [15, 16]. It can be seen from Table 2 that the activation energies (E_1) for stage 1, although somewhat higher, are consistent with those for vacancy migration [2, 8].

Table 2 Activation energies and values of process frequency factors for the stage 1, together with the correlation coefficients

Zn content in the material/ at. %	E_1 / kJ·mol^{-1}	E_2 / kJ·mol^{-1}	k_o $\times 10^9 s^{-1}$	ρ_o
30	76.7	84.2	0.7	0.99
25	78.5	94.7	1.2	0.98
20	83.6	111.4	5.0	0.98

The next step consists in adjusting a suitable law to the experimentally reacted fractions y for stage 1. A mechanism-non-invoking method will be assumed [17]. The integrated first order kinetic approach under non-isothermal conditions gives

$$\ln(1-y)^{-1} = k_o\theta \tag{1}$$

where y is the reacted fraction, k_o is the process frequency factor (also termed pre-exponential factor) and θ is the reduced time (the time at which the reactions goes to completion at an infinite temperature). Its value can be calculated from [18]

$$\theta = \frac{RT^2}{\Phi E} \exp\left(-\frac{E}{RT}\right) \tag{2}$$

where T is the temperature and R the universal gas constant. In order to calculate reduced times, the respective activation energy values were introduced in Eq. (2), thus allowing one determine θ along the temperature ranges where each peak is displayed.

Equation (1) was tested for the present data with successful results. It was possible to compute pre-exponential factors from plots of $\ln\{1/(1-y)\}$ *vs.* θ. These plots which resulted in straight lines of slope k_o are shown in Fig. 2, their values being listed in Table 2. The large values of the correlation coefficients ρ_o, computed using an ensemble of point data obtained from three DSC runs, confirm that a first-order kinetic law can be associated with stage 1 with a high degree of reliability.

The retained degree of order

The change in internal energy, in α brass alloys, can be described entirely by the first SRO parameter [19]. Hence the transformed fraction for stage 1 can be expressed as $y=(\alpha-\alpha_E)/(\alpha_{T2}-\alpha_E)$, where α_{T2} is the equilibrium first SRO parameter when stage 1 goes to completion and α_E is the value retained after quenching. The temperature dependence of α is mostly independent of the SRO model chosen [20]. We shall adopt an equilibrium Warren-Cowley parameter $\alpha=1-(p^e_{Cu-Zn})/c$, where p^e_{Cu-Zn} is the conditional probability of finding a zinc atom next to a given copper atom and c is the concentration of zinc atoms. The superscript e denotes the equilibrium value. The conditional probability will be calculated from [21].

$$p^e_{Cu-Zn} = \frac{-1 + [\{1 + 4c(1-c)(w^2-1)\}]^{1/2}}{2(1-c)(w^2-1)} \tag{3}$$

where $w^2=\exp(2W/RT)$

Boundary values for α_E can be estimated as follows. Since energy evolutions during the non-isothermal scans are due to the return of SRO and energy absorptions are due to the destruction of SRO, the degree of order present at room temperature after quenching may be specified in terms of an equivalent temperature T_E at which these degrees of order would be in equilibrium [22]. In or-

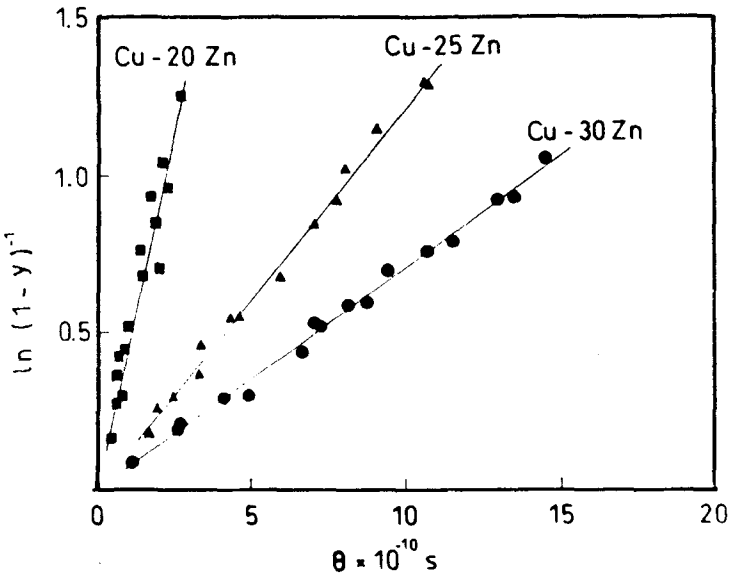

Fig. 2 Plots of $\ln\{(1-y)^{-1}\}$ *vs.* θ for αCu–Zn alloys quenched from 873 K

der to make the method straightforward, a schematic representation of a DSC trace is shown in Fig. 3. From this figure, for a given quenching temperature T_E can be calculated from a knowledge of the net absorption or evolution of energy up to some temperature at which a constant rate of destruction of order has

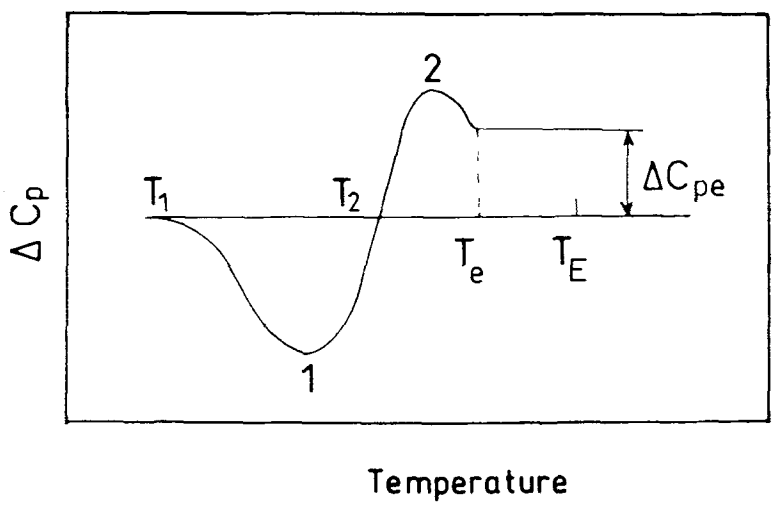

Fig. 3 DSC curves showing a schematic representation of a one-stage SRO ordering process followed by a disordering stage in a quenched alloy. T_E, may be simply specified as the temperature 1 which the equilibrium degree of order corresponding to that temperature is retained at room temperature

been attained, and the rate of absorption of energy on continuous heating above such temperature. If $\Delta H_1(T_1,T_2)$, $\Delta H_2(T_2,T_e)$ are the energies associated with the respective peaks, and $\Delta H_E=\Delta C_{pe}(T_E-T_e)$, where ΔC_{pe} and T_e represents the constant differential specific heat and the equilibrium temperature at which energy commences to be absorbed at a constant rate, one has $\Delta H_E=\Delta H_1(T_1,T_2)-\Delta H_2(T_2,T_e)$, and hence

$$T_E = T_e + \frac{\{\Delta H_1(T_1,T_2) - \Delta H_2(T_2,T_e)\}}{\Delta C_{pe}} \quad (4)$$

All relevant data and the corresponding values for α are listed in Table 3. It can be observed that the values of α are higher then those reported by Pfeiler *et al.* [23], at same temperature and same alloy.

Table 3 Values for T_2, T_E, ΔH_E, ΔC_{pe} and first SRO parameter at T_2 and T_E

Zn content in the material/at.%	T_2 / K	T_E / K	ΔH_E / kJ·mol^{-1}	ΔC_{pe} / kJ·mol^{-1}K^{-1}	$-\alpha_{T2}$	$-\alpha_E$
30	460	560.6	97	1.6	0.202	0.165
25	476	568	78	1.52	0.161	0.136
20	511	599	36.6	1.27	0.117	0.101

It can also be seen that the retained degree of order at room temperature specified by α_E and the equilibrium value α_{T2} are lower as the alloy becomes more diluted. The first short range order parameter variation *vs.* temperature is displayed in Fig. 4 using the relation:

$$\alpha = y(\alpha_{T2} - \alpha_{TE}) + \alpha_E \quad (5)$$

The value of y was experimentally obtained from each curve as $y=a_T/A$, where a_T is the reacted area to temperature T and A is the total area under stage 1. It can be noticed that the reordering process starts and also reaches the equilibrium state at lower temperatures for higher aluminum contents. All the above features are consistent with the lower availability of solute and with the decrease in atomic mobility as the solute concentration decreases.

Effect of quenching temperature

Figure 5 shows the DSC traces corresponding to specimens of Cu-30Zn quenched from the indicated selected temperatures, T_q. In these DSC curves, the temperatures T_1, T_2 and T_e were measured and α_{T2}, α_E and α_{Tq} calculated together with ΔH_1. All these data are presented in Table 4. Plots of the variation

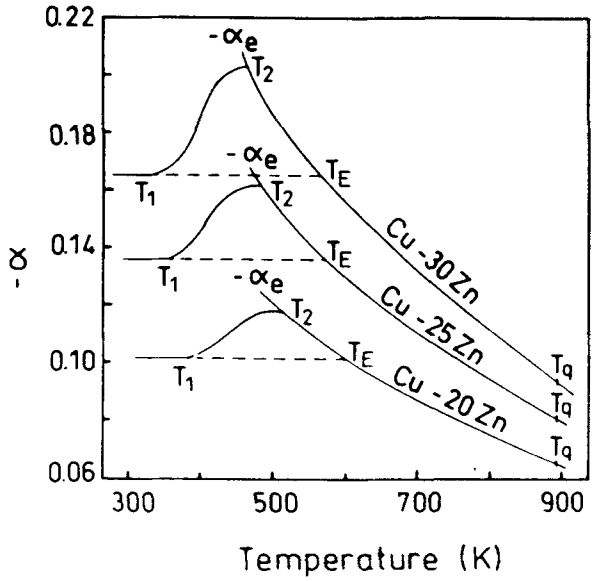

Fig. 4 Variation in the first SRO parameter for αCu–Zn alloys quenched from 873 K, at a heating rate of 0.33 Ks^{-1}. The α_e curves represent the equilibrium first SRO parameter as a function of temperature

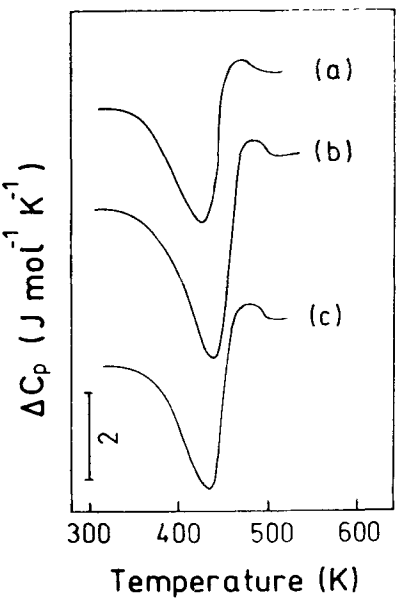

Fig. 5 DSC traces for Cu-30Zn quenched from different temperatures. (a) 673 K, (b) 873 K and (c) 1073 K. Heating rate 0.33 $deg \cdot s^{-1}$

Table 4 Values for T_q, T_1, T_2, T_e, T_E, ΔH and the first SRO parameter at T_2, T_E and T_q

	T_q /	T_1 /	T_2 /	T_e /	T_E /	ΔH_1 /	$-\alpha_{T2}$	$-\alpha_E$	$-\alpha_{Tq}$
			K			kJ·mol^{-1}			
a)	673	346	453	495	543	126	0.207	0.175	0.133
b)	873	338	460	500	560.6	155	0.202	0.165	0.093
c)	1073	332	448	498	523	130	0.211	0.179	0.078

of the first SRO parameter *vs.* temperature were made for the different quenches using Eq. (5). In these plots, which are shown in Fig. 6, the values of y were again experimentally obtained. Several points of interest arise from these results.

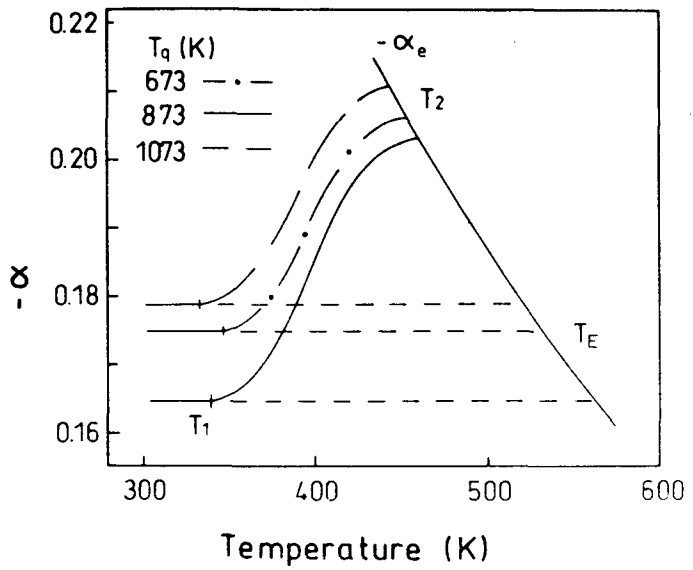

Fig. 6 Variation of the first SRO parameter for Cu-30Zn quenched from indicated temperature. The α_e curve represents the equilibrium first SRO parameter as a function of temperature

i) The degree of order present at room temperature after quenching at first decreases with quenching temperature and then increases again. Thus the maximum disorder is obtained around 873 K. For quenches above this temperature less disorder is retained, so that on quenching from 1073 K the alloy is somewhat more ordered than on quenching from 673 K.

ii) As the quenching temperature increase the degree of ordering which occurs during the quench becomes more marked. For instance, for the specimen quenched from 1073 K (α_q=–0.078), ordering during the quench changes the

degree of order from that in equilibrium at 1073 K to that in equilibrium at 523 K ($\alpha_E = -0.179$, Fig. 6). The increase in the degrees of order, which can be specified by the values of $|\alpha_E - \alpha_{T_q}|$ are 0.042/0.072/0.101 for quenching temperatures of 673/873/1073 K.

These features are of course limited by the loss of vacancies during the quench. As the SRO process is controlled by the effective jumps to produce ordering, for a quenching temperature of 673 K less vacancies migrate, contrary to what occurs at 1073 K, where the amount of reordering is increased. For 873 K the situation is intermediate. On the other hand, the higher is the quenching temperature the alloy is in a more disordered state at that temperature. A combination of these factors can explain the maximum degree of disorder found at room temperature for a quench from 873 K. These results are similar to those obtained by resistivity measurements in Au–Ag (50 at %) [24].

iii) The temperature T_2 at which the transition occurs from an evolution to an absorption of energy at the end of stage 1 results from the attainment of the equilibrium degree of order at that temperature. The temperature at which disordered commences is of course a function of the degree of disorder retained at room temperature after quenching and of the concentration of quenched-in vacancies. A consideration of these two factors explain the increase and then the decrease in the temperature at which disordering starts after quenching from the different temperatures. Thus, when quenching from 673 K the degree of disorder retained is lower as is the vacancy concentration.

Reordering occurs until the equilibrium degree of order is reached at 453 K. On quenching from 873 K more disorder is quenched-in, the vacancy concentration is still higher, so that the increased ordering during this stage enables the

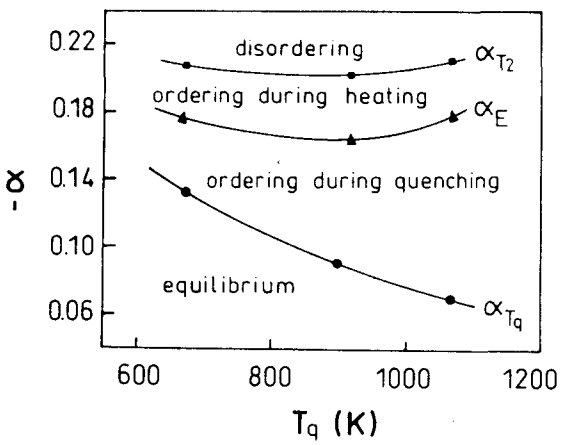

Fig. 7 Values of the first SRO parameters α_{T_q} (at the quenching temperature), α_E (retained at room temperature) and α_{T_2} (at the equilibrium temperature). The α value ranges where the indicated processes take place are also shown

equilibrium degree of order to be attained at 460 K. For the quench from 1073 K less disorder is quenched-in than for quenches from 673 K and 873 K, but the vacancy concentration is higher than for either of these temperatures, so that considerable ordering occurs and the equilibrium degree of order is reached at 448 K. These results are consistent with the increase in order during the heating process measured by $|\alpha_{T_2}-\alpha_E|$ until equilibrium is reached and also with the values of the enthalpy associated with each DSC trace, which is also a measure of the order developed. In fact $|\alpha_{T_2}-\alpha_E|=0.032/0.037/0.32$ and $\Delta H_1=126/155/130$ J·mol^{-1} for quenching temperatures of 673/873/1073 K. The already depicted features are summarized graphically in Fig. 7, where the different regions are indicated.

All the above findings indicate that reordering is controlled by non-equilibrium vacancy migration and perhaps by more complex mechanisms involving solute-vacancy binding effects. These complexes can play an important roll in the ordering process in the latter part of stage 1 and will be considered later on.

It is also worthwhile to recall that depending upon the quenching conditions in other alloy systems such us αCu–Al, the ordering process can take place in two stages [25, 26]. The first one is associated with the migration of non-equilibrium vacancies and the second one with the migration of thermal vacancies. This behavior is attributed to the fact that the effective activation energy for vacancy migration which promotes ordering, is larger than the activation energy for vacancy migration to sinks which controls its lifetime [27].

Vacancy behavior

a) Bound vacancies

Vacancy-solute binding in α brass alloys may be important regarding the effective vacancy mobility. In general the binding effect arises from two factors: size factor and electronic factor [28]. The size factor is responsible for the strain field being produced by the size mismatch for oversized solute elements such that the lattice strain so produced is minimized by vacancy-solute atom association. The electronic factor, on the contrary, is considered to be prevalent in the presence of a solute element of valency higher than that of the host element. In the case of α-brass alloys, both factors are present. Hence a non-negligible binding energy is expected in a Zn-vacancy complex. It the activation energy for vacancy formation is considered as $E_f=E_{sd}/2$, being E_{sd} the activation energy for interdiffusion, which is estimated from the Brown and Ashby correlations [29], then $E_f=91.8/94.3/96.1$ kJ·mol^{-1} for 30/25/20 at.% Zn. As all expressions relating the effective vacancy formation energy to solute-vacancy binding energy E_{v-s} are valid only for dilute alloys, interpolated values for E_f are required. For 8.0 and 5.0 at.% Zn one obtains 100.0 and 101.7 kJ·mol^{-1} re-

spectively, assuming that for pure copper $E_v^f = 106.4$ kJ·mol^{-1} [30]. The interpolated values for E_f were substituted into [31]

$$E_f = E_v^f - E_{v-s}\left\{\frac{1-12c}{12c}\exp\left(-\frac{E_{v-s}}{RT_q}\right)+1\right\}^{-1} \quad (6)$$

It can be seen that E_f is not a linear function of T_q. However, it is found experimentally through measurements of excess resistivity $\Delta\rho_a$ introduced by quenching that, for varying quench temperatures over a sufficiently narrow range of values of T_q, $d\{\ln(\Delta\rho_a)\}/d(1/T_q) \approx -E_f/R$. Iteratively calculated values of E_{v-s} for 8.0 and 5.0 at.% Zn alloys quenched from 873 K give 19.4 and 17.4 kJ·mol^{-1}. An average value of $E_{v-s} = 18.4$ kJ·mol^{-1} was obtained. Such a value considered high enough in that an important fraction of atoms might be bounded [32]. For instance, for Cu-30Zn these less mobile complexes increase the effective activation energy E_1 for vacancy migration compared with reported values for the activation energy of migration of monovacancies [2].

The effect of vacancy trapping by solute atoms may be important with respect to their thermal release in determining the bound vacancy concentration; assuming that $E_{v-s} = 5RT$ [33] in the present case give $T \leq 443$ K, which mean that the trapping effect is effectively important during the ordering process (stage 1).

It is interesting to point out also that $E_{v-s} + E_{v-s}' = 2W$ [34], E_{v-s}' being the vacancy-Cu binding energy which amounts to -24.58 kJ·mol^{-1}, indicating strong repulsion. The ordering energy, W, for Cu–Zn alloys ($W = V_{Cu-Zn} - 1/2(V_{Cu-Cu} + V_{Zn-Zn})$, where V_{i-j} is the binding energy of Cu–Zn atomic pair) was taken as $W = -3.09$ kJ·mol^{-1} [20].

b) Vacancy mobility

The mobility of vacancies influences the ordering rate in two ways. First, it controls the lifetime of vacancies and hence for the case of excess vacancies their concentration. In this respect, although the vacancies interchange alternately with atoms of either of the constituent elements copper and zinc, the two types of jump cannot be distinguished in averaging the migration rate of vacancies to sinks and the associated lifetimes. Possible coupling of vacancies to one sort of an atom is not considered.

The vacancy mobility ν_m is simply the sum of interchange frequencies with atoms of copper and zinc. Hence,

$$\nu_m = \nu_{Cu} + \nu_{Zn} \quad (7)$$

and the activation energy for vacancy migration is

$$E_m = \frac{\partial}{\partial(1/RT)} \ln\left(\frac{1}{\nu_{Cu} + \nu_{Zn}}\right) \tag{8}$$

On the contrary, the relation between these jump frequencies ν_{Cu} and ν_{Zn} and the resulting ordering rate is more complex. Clearly, not every atom jump does participate in the ordering. To evaluate the ordering rate, only Cu–Zn or Zn–Cu jumps are to be taken into account. A weighted frequency ν_m^* must be used [35]

$$\frac{1}{\nu_m^*} = \frac{1}{2Z\gamma}\left(\frac{1}{\nu_{Cu}} + \frac{1}{\nu_{Zn}}\right) \tag{9}$$

where Z (=12) is the coordination number and the value of γ is 1 and 1/7 for directional and SRO respectively [35]. Then the activation energy E_m^* associated with ν_m^* is

$$E_m^* = \frac{\partial}{\partial(1/RT)} \ln\left(\frac{1}{\nu_{Cu}} + \frac{1}{\nu_{Zn}}\right) \tag{10}$$

As a consequence, while the vacancy lifetime is determined by the faster jump, ν_{Zn}, the ordering rate is controlled mainly by the slower jump, ν_{Cu}, as it can be inferred from the results presented later. The frequencies ν_{Zn} and ν_{Cu} are related to the diffusion corresponding to radioactive tracers by [36]: $D_{Cu}=(Cv\nu_{Cu}a^2)/(1-c)$ and $D_{Zn}=(C_v\nu_{Zn}a^2)/C$, where C_v is the vacancy concentration and a the lattice parameter.

In order to compute ν_{Cu} and ν_{Zn}, D_{Cu} and D_{Zn} were evaluated by the method proposed by Beke *et al.* [37, 38], successfully applied to αCu–Al alloys [25, 26]. For the sake of brevity the results are directly listed in Table 5.

With the values of Q_{Cu}, Q_{Zn}, D_0(Cu) and D_0(Zn) and noting that

$$\nu_m = \nu_{om} \exp\left(-\frac{E_m}{RT}\right); \quad \nu_m^* = \nu_{om}^* \exp\left(-\frac{E_m^*}{RT}\right) \tag{11}$$

is obeyed from an Arrhenius plot, the values for ν_{om}, ν_{om}^*, E_m and E_m^* can be calculated from Eqs (7)–(10) by making use of Fig. 8. The results are listed in Table 6.

Computed values for ν_{om} and ν_{om}^* as well as the activation energies E_m for vacancy migration to sinks [39] are in excellent agreement with those obtained for other alloys systems [8, 25, 28]. Values for E_m^* are larger but still smaller than those obtained from the DSC curves for E_1 which determine the ordering rate. E_m and E_m^* correspond to monovacancies and in absence of bound vacancies the effective activation energies E_1 would be expected to be very close to E_m^* for

Table 5 Values of activation energies for impurity diffusion Q_{Cu}, Q_{Zn} and diffusion constants $D_0(Cu)$, $D_0(Zn)$

Zn content/ at.%	Q_{Cu} kJ/mol	Q_{Zn} kJ/mol	$D_0(Cu)$ $x10^{-4}m^2/s$	$D_0(Zn)$ $x10^{-5}m^2/s$
30	170.1	151.2	0.32	0.78
25	176.9	157.8	0.36	0.94
20	183.7	164.6	0.41	1.14

Table 6 Values for activation energies for vacancy migration and jump frequency constants

Zn content/ at.%	E_m/ $kJ \cdot mol^{-1}$	E_m^*/ $kJ \cdot mol^{-1}$	ν_{om}/ $x10^{14}s^{-1}$	ν_{om}^* $x10^{14}s^{-1}$
30	71.4	71.9	0.73	1.0
25	73.7	74.1	1.2	1.6
20	76.5	77.2	2.3	2.7

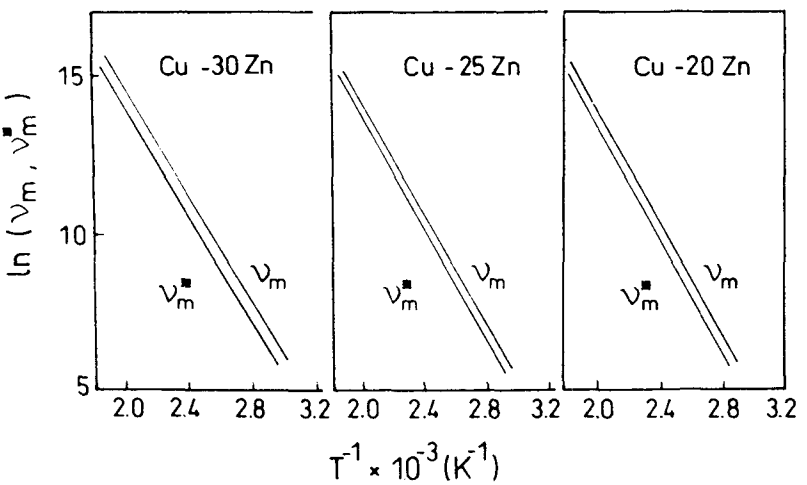

Fig. 8 Vacancy jump ν_m to sinks and vacancy jump frequency controlling the SRO rate ν_m^* against the reciprocal temperature for αCu–Zn alloys

each alloy concentration. However, it was shown previously that the influence of vacancy complexes with a lower mobility may contribute to an increase in E_1 in comparison with E_m^*. Therefore, $E_1 > E_m^* \approx E_m$ as calculated seems to be quite reasonable. The fact that $E_m^* \approx E_m$ indicates that the excess vacancy migration process is very effective in promoting order, thus explaining the existence of only one stage during anisothermal heating before equilibrium is reached.

By the other hand, one can calculate, for SRO process assisted by migration of excess vacancies, a process frequency factor [25]

$$k_o^* = \eta C_v(0)\ \nu_{om}^* / 2 \tag{12}$$

assuming that k_o^* calculated by non-isothermal techniques is the average between the initial and final values. With the values of the effective energy for vacancy formation given by $E_f = E_{sd}/2$, and considering as a first approximation that the vacancy concentration just after quench $C_v(0) = c^* \exp(-E_f/RT_q)$ being $c^* \approx 2$, one obtains $C_v(0) = 1.3\times10^{-5}/9.2\times10^{-6}/7.3\times10^{-6}$ for 30/25/20 at.% Zn, giving $k_o^* = 0.65\times10^9/0.74\times10^9/1.0\times10^9$ s, if $\eta \approx 1$. These values are in fairly good agreement with the values of k_o calculated from the DSC traces (Table 2).

The method of Beke *et al.* [37, 38] used to compute impurity diffusion coefficients allows one also to estimate the binding energy of divacancies, which can be expressed by

$$E_{2v}(c) = \lambda \alpha'(c) T_c(c) \tag{13}$$

Using $\lambda = 0.16$ [32] and the computed values for $\alpha'(c) = 71.9\times10^{-3}/70.5\times10^{-3}/69.8\times10^{-3}$ kJ·mol^{-1}K^{-1} and $T_c(c) = 1210/1240/1266$ K for 30/25/20 at.% Zn defined in Ref. [37], gives an average value of $E_{2v} = 14.0$ kJ·mol^{-1}. This value is in good agreement with those obtained for other alloy systems [25, 32].

It is interesting to notice that the binding energy of divacancies E_{2v} is lower than the binding energy of a single vacancy to a solute atom ($E_{v-s} = 18.4$ kJ·mol^{-1}). Therefore, it can assumed that the formation of divacancies can be ignored as a first approximation because a single vacancy has more chance to encounter a solute atom than another vacancy.

Conclusions

The investigation by differential scanning calorimetry of the ordering process in αCu–Zn alloys leads to the following conclusions:

a) Rising temperature experiments are better interpreted in terms of a homogeneous SRO than a heterogeneous DO model.

b) Under non-isothermal heating after quenching as described above, SRO takes place in one stage, stage 1 at low temperatures. The SRO kinetics until equilibrium is attained become faster as Zn content increases. Stage 1 ordering is assisted by the migration of excess vacancies.

c) Effective activation energies for stage 1 are consistent with those for vacancy migration controlling the ordering rate. Activation energies for vacancy

migration controlling their associated lifetime resulted in similar values. Thus, excess vacancy migration is very effective in producing ordering.

d) The number of less vacancy-solute complexes may be important in these alloys. A solute-vacancy binding energy of 18.4 $kJ \cdot mol^{-1}$ was estimated.

e) The process frequency factor values are in agreement with those expected from the development of SRO during stage 1.

f) Finally, the assessment of non-isothermal SRO behavior in terms of the first SRO parameter computed using DSC traces, allows to evaluate quantitatively the retained degree of order after quenching and the ordering features during anisothermal heating, thus enables to extend the capabilities of differential scanning calorimetry procedures.

* * *

The authors wish to thank the Fondo Nacional de Desarrollo Científico y Tecnológico (FONDECYT), Project N° 1950566, and the Departamento de Ingeniería de los Materiales-IDIEM, Facultad de Ciencias Físicas y Matemáticas de la Universidad de Chile for financial support.

References

1 R. Poerschke and H. Wollenberger, J. Nucl. Mater., 74 (1978) 48.
2 E. Balanzat and J. Hillairet, J. Phys. F. Met. Phys., 11 (1981) 1977.
3 L. M. Clarebrough and M. H. Loretto, Proc. R. Soc. A, 257 (1960) 326.
4 L. M. Clarebrough, M. E. Hargreaves and M. H. Loretto, Proc. R. Soc. A, 261 (1961) 500.
5 D. T. Keating, Acta Metall., 2 (1954) 885.
6 R. Feder, A. S. Nowick and D. B. Rosenblatt, J. Appl. Phys., 29 (1958) 984.
7 H. M. Otte, J. Appl. Phys., 33 (1961) 1436.
8 M. Halbwachs, D. Beretz and J. Hillairet, Acta Metall., 27 (1979) 463.
9 R. Poerschke and S. Mantl, Radiat. Eff., 41 (1979) 61.
10 D. Trattner and W. Pfeiler, J. Phys. F. Met. Phys., 13 (1983) 739.
11 W. Schüle, Mater. Sci. Forum, 97–99 (1992) 223.
12 L. Reinhard, B. Schönfeld, G. Kostorz and W. Bührer, Z. Metallkd., 84 (1993) 251.
13 M. Van Rooyen, J. A. Sinte Maartensduk and E. J. Mittemeijer, Metall. Trans. A, 19 (1988) 2433.
14 H. E. Kissinger, Anal. Chem., 28 (1957) 1702.
15 A. Varschavsky and E. Donoso, Metall. Trans., 15A (1984) 1999.
16 A. Varschavsky and E. Donoso, J. Mater. Sci., 21 (1986) 3837.
17 K. N. Niman, J. Thermal Anal., 35 (1989) 1267.
18 C. Sandu and R. Singh, Thermochim. Acta, 159 (1990) 267.
19 N. Kuwano, I. Ogata and T. Eguchi. Trans. Jpn. Met., 18 (1977) 87.
20 W. Pfieler, Acta Metall., 36 (1988) 2417.
21 S. Radelaar, J. Phys. Chem. Solids, 31 (1970) 219.
22 S. Matsuo and L. M. Clarebrough, Acta Metal., 11 (1963) 1195.
23 W. Pfeiler and R. Reihsner, Phys. Status Solidi A, 97 (1986) 377.
24 A. Beukel van den, P. C. J. Coremans and M. M. A. Venhoef, Phys. Stat. Sol., 19 (1967) 177.
25 A. Varschavsky and E. Donoso, Mater. Sci., Eng., A145 (1991) 95.
26 A. Varschavsky, Thermochim. Acta, 203 (1992) 391.
27 A. Varschavsky and M. Pilleux, Mater. Letts., 17 (1993) 364.
28 A. K. Mukhopdhyay, G. J. Shiflet and E. A. Starke, Scr. Metall. Mater., 24 (1990) 307.

29 A. M. Brown and M. F. Ashby, Acta Metall., 28 (1980) 1085.
30 H. Kimura and R. Maddin, Quench Hardening in Metals, North-Holland, Amsterdam 1971, p. 17.
31 J. I. Takamura, M. Doyama and H. Kisitani, Point Defects and Defect Interactions in Metals, North-Holland, Amsterdam, 1982, p. 452.
32 S. Özbilen and H. M. Flower, Acta Metall., 37 (1989) 2993.
33 L. K. Mansur, Acta Metall., 29 (1981) 375.
34 F. W. Schapink, Philos. Mag., 12 (1965) 1055.
35 A. Caplain and W. Chambron, Acta Metall., 25 (1977) 1001.
36 M. Halbwachs and J. Hillairet, Phys. Rev. B, 18 (1978) 4927.
37 D. L. Beke, I. Godény, F. J. Kedves and G. Erdélyi, J. Phys. Chem. Solids, 40 (1979) 543.
38 D. L. Beke, I. Uzonyi and F. J. Kedves, Philos. Mag., 44 (1981) 983.
39 V. P. Fadin and V. Ye Panin, Fiz. Met. Metalloved., 14 (1962) 517.

Zusammenfassung — Die Kinetik-Nahordnung (short-range-order, SRO) in abgeschrecktem Cu-30 At%Zn, Cu-25 At%Zn, Cu-20 At%Zn zeugt mit steigendem Zn-Gehalt von anwachsender Atombeweglichkeit. Anhand der DSC-Kurven wird darauf geschlossen, daß die Ordnung in einem Stadium gefestigt wird, unterstützt durch einen Gitterleerstellenüberschuß. Bei Erhöhen der Abschrecktemperatur erfolgt während des Abkühlens von der Abschrecktemperatur eine erhebliche Rückordnung. Die Änderung des SRO nichtisothermen Verhaltens mit der Abschrecktemperatur und der Zusammensetzung wird interpretiert mit der Atombeweglichkeit und dem Grade der Unordnung zusammen mit der Konzentration der durch das Abschrecken zurückgehaltenen Gitterleerstellen. Die Aktivierungsenergien, welche die mittlere Lebensdauer der Gitterleerstellen und die Ordnungsgeschwindigkeit bestimmen waren sehr ähnlich, was darauf hinweist, daß die Beweglichkeit der Gitterleerstellen beim Aufbau der Nahordnung sehr effektiv ist. Diese Aktivierungsenergien sind etwas niedriger als die effektiven Energien, welche die Kinetik des Prozesses anhand der DSC-Kurven bestimmen, was darauf hinweist, daß die Gegenwart von gelöster Stoff-Gitterleerstellen Komplexen bei steigender Zn-Konzentration wichtig werden kann. Dieses Merkmal wird durch eine Schätzung der gelöster Stoff-Gitterleerstelle Bindungsenergie bestätigt. Weiterhin wird darauf geschlossen, daß die Bildung von Doppelgitterleerstellen in den untersuchten Legierungen unwahrscheinlich ist.